Molybdenum Disulfide MoS2 and the q-BWF line shapes (Raman Spectroscopy)

Molybdenum Disulfide MoS_2 and the q-BWF line shapes (Raman Spectroscopy)

Amelia Carolina Sparavigna

Department of Applied Science and Technology, Polytechnic University of Turin, Italy

Email: amelia.sparavigna@polito.it

RRUFF database is proposing the Raman spectra of two molybdenum disulfide MoS_2 samples. Here we show the q-BWF fitted functions to the E_{2g} and A_{1g} Raman bands of these samples. The q-BWF functions are generalizing the Breit-Wigner-Fano line shape in the framework of the q-exponential function proposed by Constantino Tsallis and his statistics. The fitted q-BWF functions to pyramid and monolayer Raman spectra by Fabbri et al., 2022, are also proposed. Some review of Raman spectroscopy of MoS_2 is proposed too.

Keywords: Raman spectroscopy, Spectrum decomposition, q-Gaussian Tsallis lines, Breit-Wigner-Fano line shape, q-BWF line shape, Molybdenum disulfide.

Introduction

Recently, we considered how the Raman spectra of graphene and graphene oxide appear when compared to graphite. In the review we mentioned the Breit-Wigner-Fano (BWF) line shape, that Ferrari and Robertson, 2000, told suitable to represent the G band of carbonaceous materials. BWF is a modified Lorentzian function used to consider asymmetry and Fano resonance (see please Miroshnichenko et al, 2010, about Fano theory and model). For instance, Hasdeo et al., 2014, used the "Breit-Wigner-Fano line shapes in Raman spectra of graphene", because of the "interference effect between the phonon spectra and the electron-hole pair excitation spectra" (Hasdeo et al., 2014). Let us stress that asymmetry can be obtained also by using a split-Lorentzian function for instance. What is characterizing the BWF function is the presence of a "shape resonance", as shown in the Fig.2 by Bianconi, 2003, or, as given elsewhere (Tanwar et al., 2022), of the "dip" of antiresonance.

In 2023, we proposed for Raman spectroscopy a generalization of the Lorentzian profile as a q-Gaussian line shape. The q-Gaussian is a function based on the Tsallis q-form of the exponential function (Tsallis, 1988). This generalized exponential is characterized by a q-parameter and when q is equal to 2, we have the Lorentzian function. If q is close to 1, we have a Gaussian function (this is the reason why the Tsallis function is also called "q-Gaussian"; here, it would be better to consider it as a q-Lorentzian). For values of q between 1 and 2, we have a bell-shaped function with power-law wings ranging from Gaussian to Lorentzian tails. As shown on many occasions, the q-Gaussian is suitable for fitting Raman spectra (from those given in SSRN to the SERS cases, and others). However, we can use the q-exponential to also generalize the split-Lorentzian function (see Appendix), and to turn the Breit-Wigner-Fano into a q-BWF function. Let us write the BWF as follow:

$$BWF = C\frac{\left[1-\xi\gamma^{1/2}(x-x_o)\right]^2}{\left[1+\gamma(x-x_o)^2\right]}$$

When parameter ξ is zero, BWF becomes a Lorentzian function. Therefore, it is easy to turn BWF into a q-BWF function:

$$\text{q-BWF} = C\left[1-\xi\gamma^{1/2}(q-1)^{1/2}(x-x_o)\right]^2\left[1+(q-1)\gamma(x-x_o)^2\right]^{1/(1-q)}$$

Please consider that in literature about Fano resonance (or Fano interference) the parameter ξ is often given by 1/q (and with an opposite sign). Here the q-parameter is related to the Tsallis statistics.

Having obtained good results with q-Gaussians for graphite and carbonaceous materials, and because of some previous investigations using the q-BWF to include the phonon confinement in the Raman spectrum, here we start applying q-BWF line shapes to the Raman spectroscopy of naturally occurring van der Waals (vdW) heterostructures. Of them, graphite and molybdenite are the best known naturally occurring materials (Frisenda et al., 2020). It was the exfoliation of these two natural van der Waals minerals, that "shaped a whole new field of research", that is that of the 2D materials (Frisenda et al., 2020). Today, most materials are synthetic, but nature is providing plenty of van der Waals materials that can have relevant applications. Let us start considering the molybdenite, that is, the molybdenum disulfide, MoS_2.

RRUFF database (Lafuente et al., 2015) is proposing the Raman spectrum of two molybdenum disulfide samples. Here in the following we show the q-BWF fitted functions to the E_{2g} and A_{1g} Raman bands of them. We will also apply q-BWFs to the spectra of MoS_2 pyramids and monolayers (Fabbri et al., 2022). Some review of Raman spectroscopy of MoS_2 is also proposed.

RRUFF Molybdenite

We have two spectra: R050209 and R060124 . Samples are: Molybdenite from Boss Mountain mine, Hendrix Lake, British Columbia, Canada (Source: Lloyd Twaites, Owner: RRUFF), Measured Chemistry: Mo1.00S2.00, and Molybdenite from Crown Point mine, near Chelan, Washington, USA, (Source: University of Arizona Mineral Museum 11966, Owner: RRUFF), Measured Chemistry: Mo1.00S2.00. Samples were unoriented and the instrument was Thermo Almega XR 532nm @ 100% of 150mW.

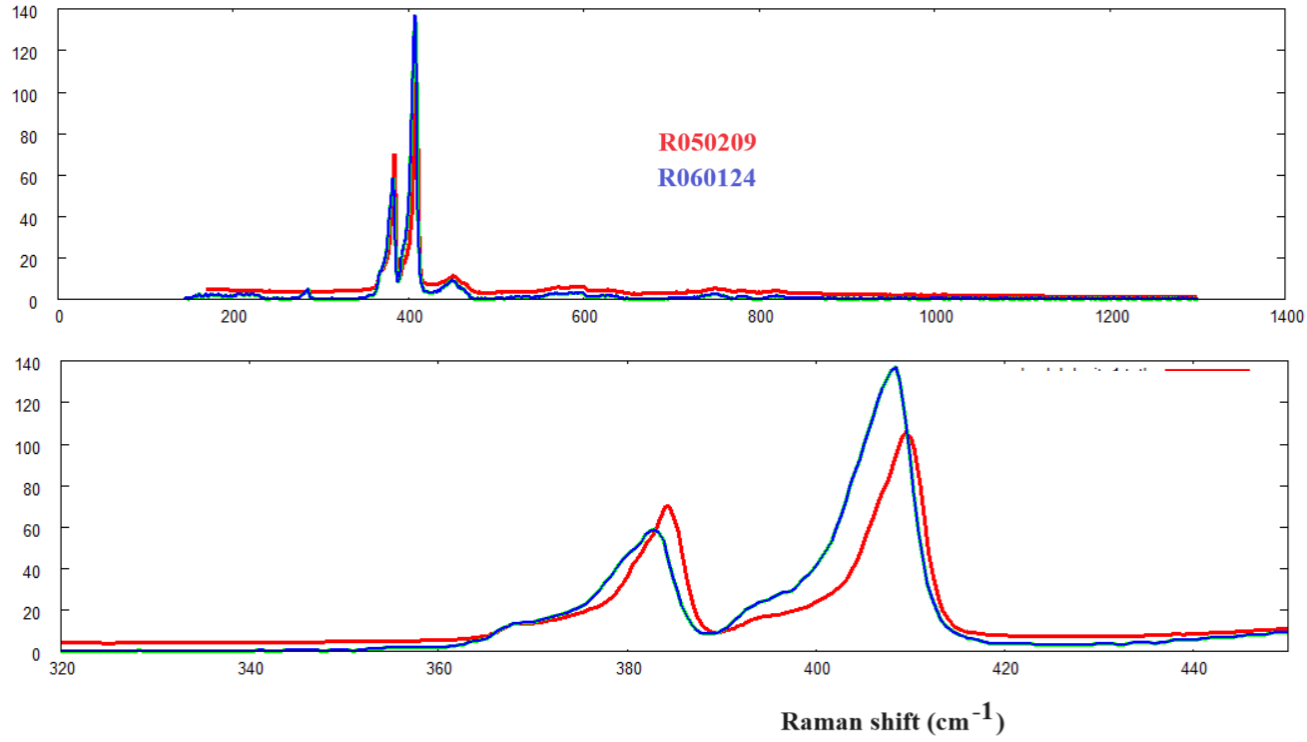

Fig.1 : Raman spectra of Molybdenum Disulfide from RRUFF.

In the lower part of the Figure 1, we can see the two main peaks of molybdenite. In the Application Note by Angela Flack, 2022, the band are given as E_{2g} band at 385 cm^{-1} and A_{1g} band at 405 cm^{-1}. "The E_{2g} band is due to in-plane

vibrations, and the A_{1g} band attributed to out-of-plane vibrations" (Flack, 2022). Note the asymmetry of the peaks. We could use several fitted Lorentzians and Gaussians or q-Gaussians to decompose the peaks, but here we want to test the use of asymmetric q-Gaussians. Let us start from two q-BWF functions. To show the decomposition, let us use Fityk software (Wojdyr, 2010). Fityk is a curve fitting and data analysis application, free and open source. It can perform a Levenberg-Marquardt algorithm, among other best fit algorithms. The function of merit is the weighted sum of squared residuals (WSSR), also called chi square. Fityk has several built-in functions but allows to execute a script with user-defined functions (see in the Appendix how we can define in Fityk q-Gaussian, split-q-Gaussian and q-BWF functions).

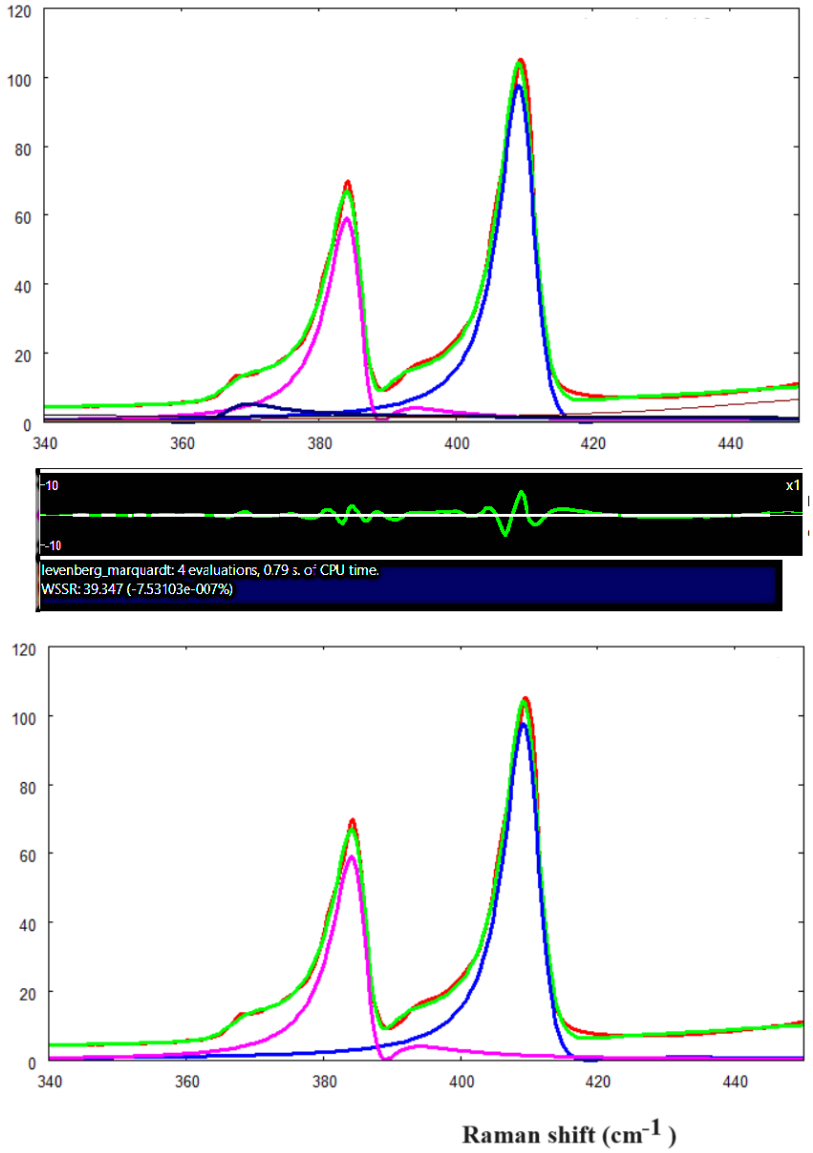

Fig.2: The red line is giving the RRUFF data R050209. The fitted green line is the sum of the q-BWF components of spectrum decomposition. To fit the data given in the upper panel of the Figure 1, we used 8 q-BWF functions. Here we show only the part of the spectrum from 340 to 450 cm^{-1}. In the lower panel, just the two main components are given; the blue and the magenta lines have q(blue)=1.60 and q(magenta)=1.50. In the middle, the resulting misfit is proposed. The misfit is the difference between data (red) and the fitted curve (green).

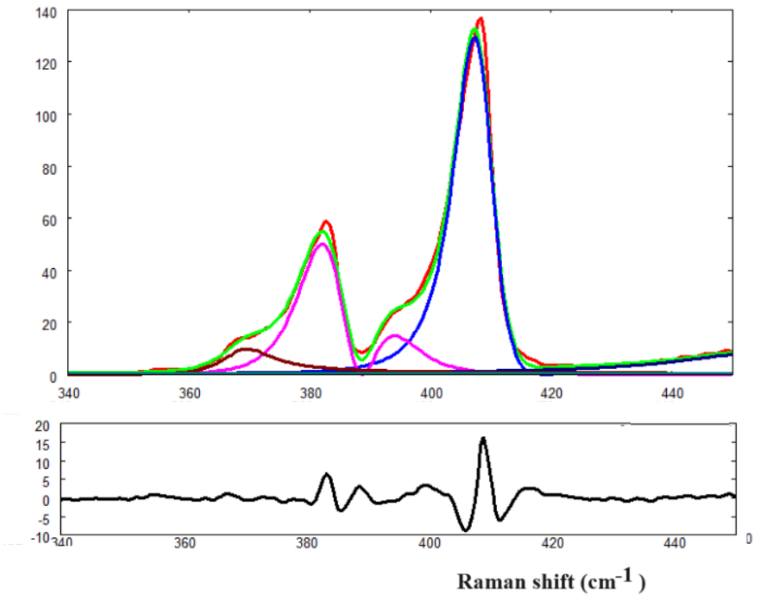

Fig.3: The red line is giving the RRUFF data R060124. The green line is giving the sum of q-BWF components. In this case too, to fit the data given in the upper panel of the Figure 1, we used 8 q-BWF functions. Here we show only the part of the spectrum from 340 to 450 cm^{-1}. The lower part of the figure is giving the misfit.

From the Figures 2 and 3, it seems that a q-BWF component function is producing a peak and a related satellite small peak (we can easily see this fact observing the magenta lines). Alternatively, we could use the split-q-Gaussian functions, which are asymmetric too, but we need to add further components, to generate the satellite peaks. Using split-q-Gaussians for fitting, Figure 3 turns into Figure 4.

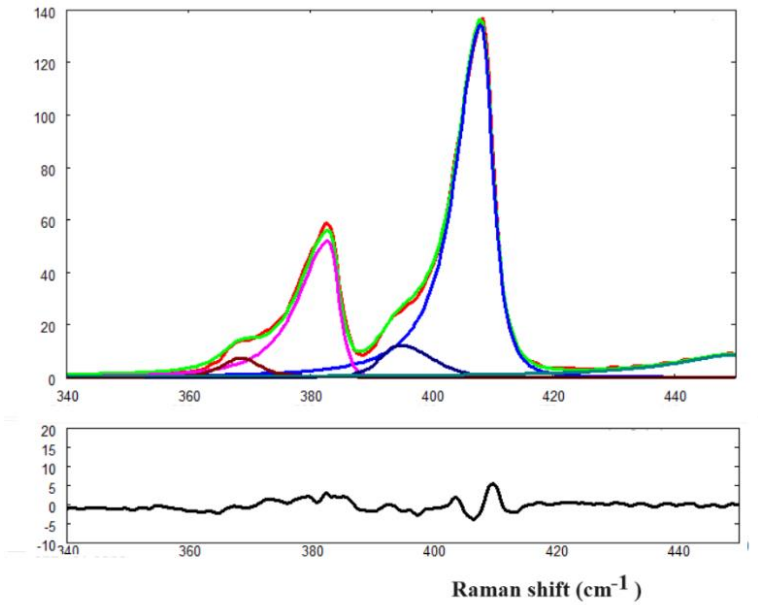

Fig.4: The red line is giving the RRUFF data R060124. In this case, to fit to data given in the upper panel of the Figure 1, we used split-q-Gaussians functions. Here we show only the part of the spectrum from 340 to 450 cm^{-1}.

Here we can repeat the observation made by Ferrari and Robertson, 2000, and proposed in the review about graphene and graphene oxide: to compare *different fitting parameters* of a Raman spectrum, it is fundamental the knowledge of *the used fitting procedures*. Once we have decided the number of components and their line shapes, we can compare parameters obtained from a set of Raman measurements. Moreover, *there is no a priori reason to choose a particular function to fit the spectrum*. Let us stress once more that Ferrari and Robertson suggested the BWF line shape for the G band in carbonaceous materials.

In the previous Figures, we proposed two best fit approaches, one based on q-BWF lines, the other on split-q-Gaussians. In the last case, increasing the number of components to describe a single band we can reduce the misfit.

Review (Phonons)

The RRUFF database is proposing Raman spectra of natural samples. The natural Molybdenum Disulfide is given as a 2H-MoS_2 crystal in the hexagonal phase. The material is a semiconductor, characterized by an indirect band gap of 1.2 eV (hqgraphene). The purity is enhanced in synthetic MoS_2. "Monolayer MoS_2 has a band gap of ~1.8 eV. … MoS_2 belongs to the group-VI transition metal dichalcogenides (TMDC)" (hqgraphene).

"Compared with graphene, 2H-MoS_2 possesses a non-zero bandgap and thus has an unlimited potential for electronic, spintronic, and optoelectronic applications" (Cao and Chen, 2019). Therefore, the study of "phonon scattering mechanisms is crucial to its device applications because the heat flow and transport are the basic processes functioning at various temperatures". Cao and Chen, 2019, have experimentally studied the temperature dependence of frequency and linewidth of the Raman peaks from 2.2 to 1000 K. "The cubic anharmonicity is found to be dominant at low temperatures, and quartic anharmonicity predominates at high temperatures" (Cao and Chen, 2019).

Of the two-dimensional materials, "one of the most exposed … is graphene", (Cao and Chen, referring to Novoselov et al., 2004), "which updates the interest in inorganic materials with its unique electronic and optical applications and high mobility" (Cao and Chen, and references therein). In graphene, "the absence of the bandgap is a limitation for its electronic applications, especially as transistors. In contrast, the transition-metal dichalcogenides (TMDs), quasi-2D materials …, possess non-zero bandgaps that could also be tuned" (Cao and Chen and reference therein). A largely investigated TMD is 2H-MoS_2. The reported experiments show the mobility of its monolayers "several times larger than traditional thin silicon films and graphene nanoribbons". The absence of inversion symmetry induces a "strong coupling of spin and valley degrees of freedom", so that 2H-MoS_2 is a "good candidate for various valley electronic and optoelectronic applications". Moreover, the strong spin-orbit coupling gives to 2H-MoS_2 the possibility of being used in spintronics (see Cao and Chen and references therein).

Cao and Chen investigated the lattice anharmonicity as a function of temperature using the Raman spectroscopy, a "tool which can directly provide a great deal of information about the optical phonon near the center of the Brillouin zone". Information is coming from the peak frequency and FWHM (full width at half maximum). Cao and Chen note that anharmonicity has been widely investigated on silicon and other 2D-materials by means of the temperature dependence of the Raman spectra, but for 2H-MoS_2, it "was reported sparsely". Cao and Chen used a synthetic sample, collecting the Raman spectra "with a laser power down to 1.0 mw *to avoid laser the heating effect*. The *heating effects are quantified by the ratio* of the anti-Stokes to Stoke Raman intensity at room temperature and found to be 3–12 K". The phonon modes in 2H-MoS_2 are $A_{1g} + 2B_{2g} + E_{1g} + 2E_{2g} + 2A_{2u} + B_{1u} + 2E_{1u} + E_{2u}$. The Raman active modes are A_{1g}, E_{1g}, E^1_{2g}, and E^2_{2g}. "In TMDs, the E_{1g} mode is always weak due to its small scattering cross section" (Cao and Chen, mentioning Wang et al., 2012). The Raman peaks are at (cm^{-1}): 34.7 (E^2_{2g}), 385.6 (E^1_{2g}), 410.9 (A_{1g}). The spectra at room temperature proposed by Cao and Chen agree "very well with previous publications" (Cao and Chen, mentioning Cao et al., 2018, Thripuranthaka et al., 2014, Pawbake, et al., 2016).

Cao and coworkers, 2018, "in some Raman experiments", "observed Raman-forbidden modes above the position of the A_{1g} mode, which [the researchers] tentatively assigned to out of plane A_{2u} and B_{2g} infrared and inactive modes", according to Molina-Sánchez and Wirtz, 2011. Molina-Sánchez and Wirtz proposed ab-initio calculations of the phonon dispersions in the case of single-layer and bulk MoS_2 and WS_2, exploring the Raman active modes A_{1g} and E^1_{2g} and how they depend on the number of layers. "In agreement with recent Raman spectroscopy

measurements [C. Lee et. al., ACS Nano 4, 2695 (2010)] [Molina-Sánchez and Wirtz] find that the A_{1g} mode increases in frequency with increasing layer number while the E^1_{2g} mode decreases. [Molina-Sánchez and Wirtz] explain this decrease by an enhancement of the *dielectric screening* of the long-range Coulomb interaction between the effective charges with growing number of layers. This decrease in the long-range part over-compensates the increase of the short-range interaction due to the weak inter-layer interaction" (Molina-Sánchez and Wirtz, 2011).

Lee and coworkers, 2010, considered MoS_2 single and few-layer thickness samples on SiO_2/Si substrate, studied by means of Raman spectroscopy. "Two Raman modes, E^1_{2g} and A_{1g}, exhibited *sensitive thickness dependence*, with the frequency of the former decreasing and that of the latter increasing with thickness. The results provide a *convenient and reliable means for determining layer thickness with atomic-level precision*. The opposite direction of the frequency shifts, which cannot be explained solely by van der Waals interlayer coupling, is attributed to Coulombic interactions and possible stacking-induced changes of the intralayer bonding" (Lee et al., 2010).

D_{2h}	D_{6h}	Character	Direction	Atoms	(cm^{-1})
-	E^2_{2g}	Raman	In-plane	Mo+S	35.2
A_1	A_{1g}	Raman	Out-of-plane	S	412.0
E'	E^1_{2g}	Raman	In-plane	Mo+S	387.8
E''	E_{1g}	Raman	In-plane	S	288.7

Table I - Adapted from Molina-Sánchez and Wirtz, who considered Wieting and Verble, 1971. The table contains the phonon symmetry representations of single-layer (point group D_{3h}) and bulk (point group D_{6h}) of MoS_2 for modes which are Raman active.

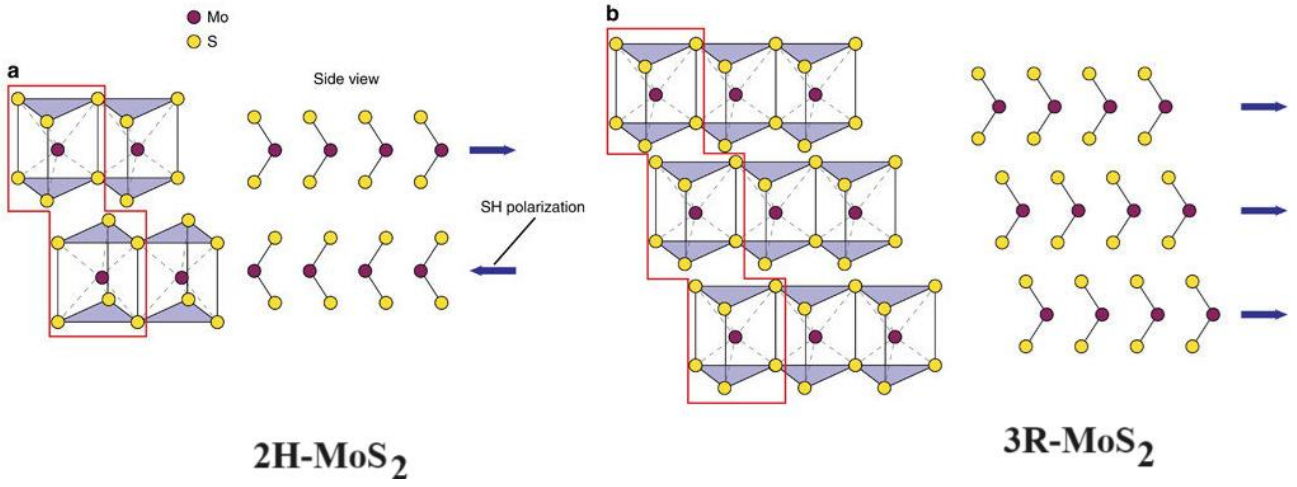

Fig. 5: The crystal structure of 2H and 3R-MoS_2 as shown in the Fig.1 by Zhao et al., 2016 (CC BY-NC-SA 4.0 DEED). Part (a) on the left is the structure of 2H-MoS_2 (the unit cell is outlined in red). "The Mo atoms are hexagonally packed within each layer and trigonal prismatically coordinated with S atoms on the top and bottom. The side projection shows the flipped orientation of each layer and the anti-parallel orientation of the SH dipoles that allow for SHG" (Zhao et al., 2016). SHG means Second Harmonic Generation. The part (b) on the right shows the structure of 3R-MoS_2. "Individual layers are identical to the 2H structure, however the unit cell and bulk crystal are non-centrosymmetric" (see in Zhao et al., 2016, the discussion of second-harmonic generation in Molybdenum Disulfide).

Polytypism

The Figure 5 shows the 2H and the 3R lattices of MoS_2. Lee et al., 2016, considered the "Raman signatures of polytypism in molybdenum disulfide". In the graphical abstract, it is possible to find a top view of the two lattices. "Since the stacking order sensitively affects various physical properties of layered materials," it is important to have an accurate determination of it. "Because 2H-molybdenum disulfide (MoS_2) is most common in nature, most studies so far have focused on 2H-MoS_2. However, [Lee and coworkers] found that the 2H, 3R, and mixed stacking sequences exist in few-layer MoS_2 exfoliated from natural molybdenite crystals. … The Raman signatures of different polytypes are investigated by using 3 different excitation energies … The low-frequency breathing and shear modes show *distinct differences for each polytype whereas the high frequency intra-layer modes show little difference*." (Lee et al., 2016). "The main E^1_{2g} and A_{1g} modes are observed at ~383 and ~407 cm^{-1}, respectively, for both polytypes". As in the Table given above, the two modes are due to "intra-layer vibrations along the in-plane or out-of-plane directions, respectively" (Lee et al., 2016). "There is no *significant difference in the intra-layer* vibration modes, which implies that each constituent layer is almost identical for both polytypes". This result by Lee and coworkers is in good agreement with previous Raman results on synthetic 3R-MoS_2 (Lee et al. are mentioning Suzuki et al., 2014).

Suzuki and coworkers used the "3R polytype crystal, which has a non-centrosymmetric structure" instead of the "conventional centrosymmetric 2H form". The 3R stacking was compared by Suzuki et al. with the 2H stackings. "To estimate the thickness of micromechanically cleaved MoS_2 samples [Suzuki and coworkers] performed micro-Raman spectroscopy experiments, in particular focused on the frequency difference between E^1_{2g} and A_{1g} modes, and atomic force microscopy (AFM)". For the 2H-stacking case, it was empirical established a correlation between the splitting of E^1_{2g} and A_{1g} modes and the number of layers, that Suzuki and coworkers determined by means of AFM. The researchers "found a similar relation holds for 3R stacking, *even quantitatively*" (Suzuki et al., 2016).

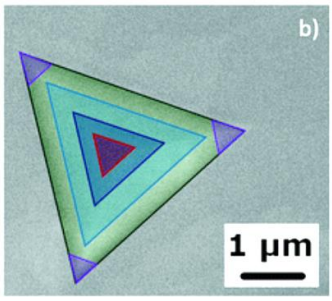

Fig. 6: Right panel of the Fig. 6 in the article by Negri et al., 2022. The image is showing a SEM micrograph of a MoS_2 pyramid, with highlighted regions in color code.

MoS_2 Pyramids

Fabbri et al., 2022, studied the "Raman and photoluminescence of MoS_2 flakes and pyramids". A data set is given in Zenodo, https://doi.org/10.5281/zenodo.5866629, Creative Commons Attribution 4.0 International. Data are used in "Excitonic absorption and defect-related emission in three-dimensional MoS_2 pyramids" by Negri et al., 2022, Open Access, CC BY 3.0 DEED. "Among the possible three-dimensional structures, MoS_2 pyramids have demonstrated promising properties for light emission, non-linear optics, such as second-harmonic generation, and ferromagnetism" (Negri et al., 2022).

"The Raman spectroscopic analysis *confirms the bulk nature* of the pyramid; in fact, the MoS_2 E_{2g} and A_{1g} Raman modes appear at 381.7 cm^{-1} and 406.6 cm^{-1}, with a separation of 24.9 cm^{-1}, which is indicative of bulk MoS_2 (see references in Negri et al.). The surrounding triangular structure is in the monolayer form; in fact, the E_{2g} and A_{1g} modes, set at 382.8 cm^{-1} and 403.3 cm^{-1} respectively, have a 20.5 cm^{-1} separation, a signature of monolayer MoS_2. In addition, the ratio between the MoS_2 mode intensity and the silicon peak confirms the bulk nature of the pyramid. It is worth noting that the E_{2g}/A_{1g} intensity ratio can give additional insights" (Negri et al., 2022).

In the following Figs.7 and 8, we use the Raman spectra given in Zenodo, and the q-BWF line shapes to fit them.

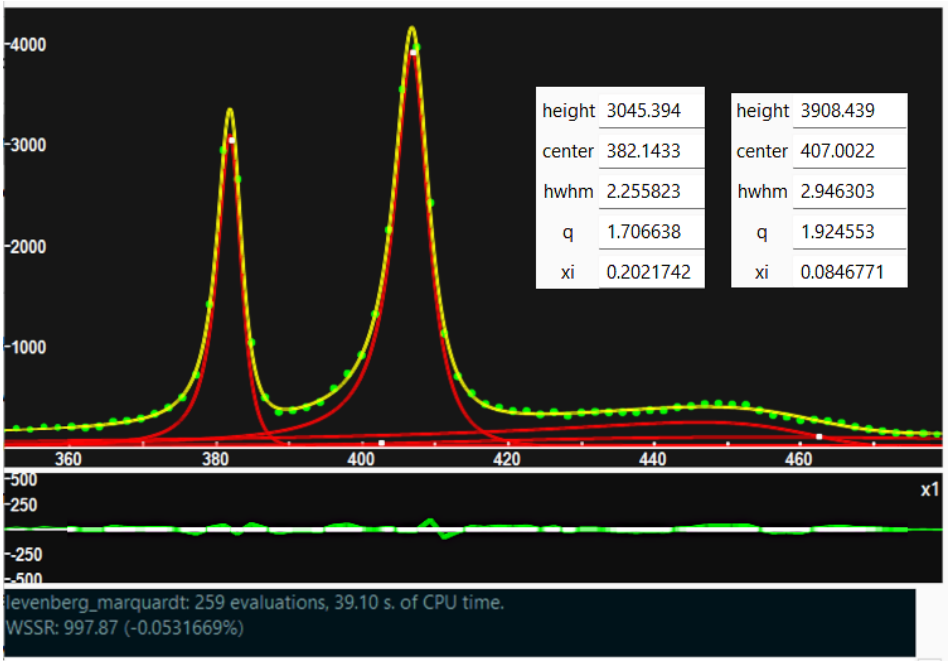

Fig. 7(a): The image is giving a screenshot of Fityk, where we used a script to define the q-BWF functions. The data (green dots) are those of the Raman spectrum of a MoS_2 pyramid available in Zenodo, https://doi.org/10.5281/zenodo.5866629. The q-BWF components are in red, and the sum of the components in yellow. The parameters of the two main q-BWFs of pyramid are given in the figure. Note the values of q being 1.71 and 1.92 for the two q-BWF functions related to MoS_2.

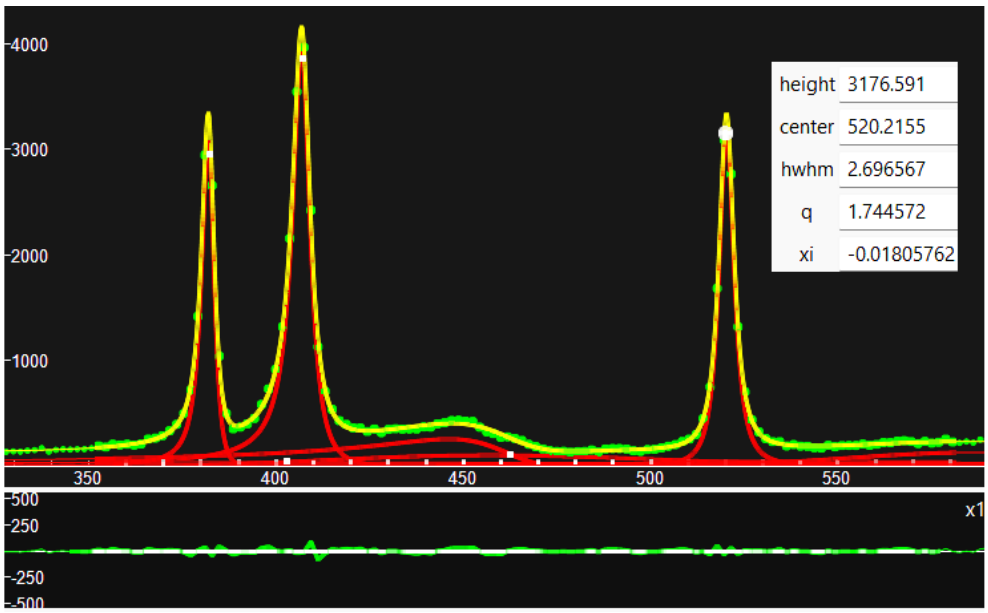

Fig. 7(b): The same as in the Figure 7(a). The screenshot is given to show the silicon peak too. Its "xi" value is small. This means that the peak is almost symmetrical.

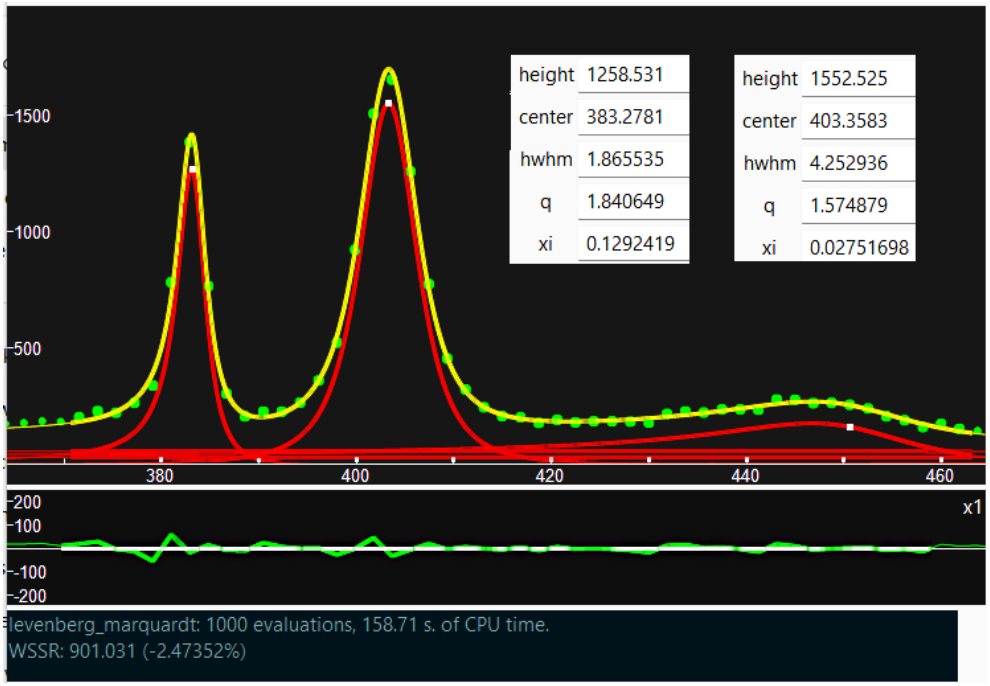

Fig. 8(a): The image is giving a screenshot of Fityk. The data are those of the Raman spectrum of a MoS_2 monolayer available in Zenodo, https://doi.org/10.5281/zenodo.5866629. The parameters of the two main MoS_2 q-BWFs are given in the figure.

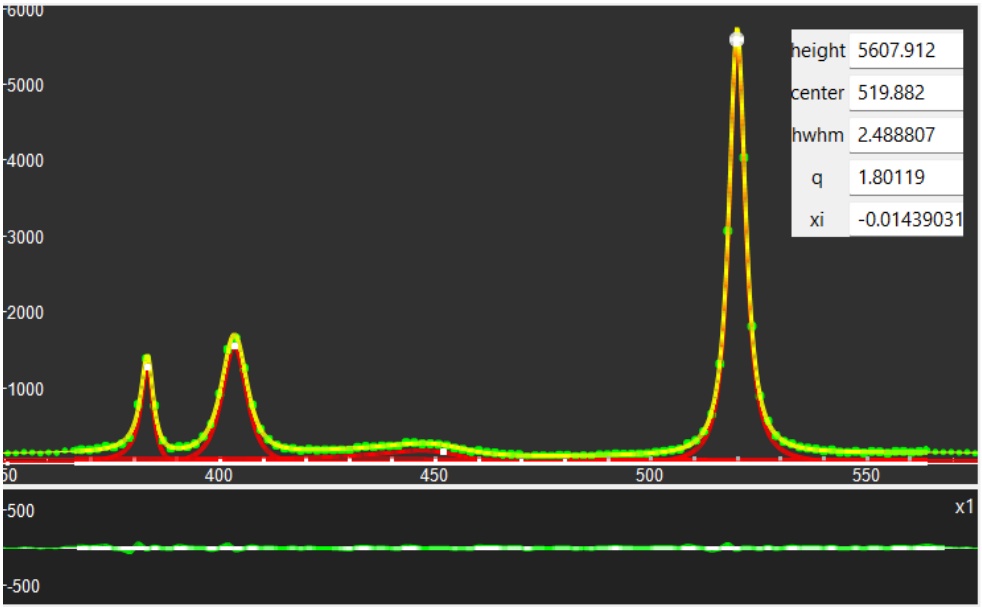

Fig. 8(b): The same as in the Figure 8(a). The screenshot is given to show the silicon peak too. It is close to be a Lorentzian peak.

From the Figures 7 and 8, we can see the very good agreement between the data and the fitted curves. Let us stress that the components of the decomposition of the spectrum are q-BWF functions. Beside the asymmetry, please note the fact that the q-parameters, characterizing the q-Gaussian approach, are different from value q=2, which is corresponding to a Lorentzian function. Another relevant fact is that the tails of the q-BWF components contribute in a sensitive manner to the resulting fitted spectrum.

Review (pressure, temperature and defect effects)

"Molybdenum disulfide (MoS_2) is a typical transition metal dichalcogenide and it has attracted considerable attention from researchers because of its unique and tunable optical, electronic, and mechanical properties. MoS_2 has a wide range of industrial applications, including *as a solid lubricant material in aerospace technology* and as *a catalyst for complex hydrocarbon dehydrogenation*. … Research into the effects of *high pressure* on MoS_2 has been conducted for several decades. In 1982, the dependence of the A_{1g} and E_{2g} modes in 2H–MoS_2 layer materials on the pressure was investigated … Theoretical research indicates that the MoS_2 monolayer and semiconductor bilayers will gradually undergo *metallization* as the pressure increases" (Tang et al. 2021, and references therein). Tang and coworkers measured high pressure Raman spectra of 2H–MoS_2 from spectra from 0 to 40 GPa (Stokes Raman) and from 0 to 31.4 GPa (anti-Stokes Raman).

Najmaei et al., 2012, considered the "thermal effects on the Raman spectra of molybdenum disulfide with thicknesses ranging from bulk to monolayer". The researchers "quantitatively determined the *laser-induced heating effects on the peak position* and the linewidth of the Raman spectrum. [Najmaei and coworkers] found considerable thickness-dependent red-shifts as well as line-width changes for both E^1_{2g} and A_{1g} vibrating modes *as laser power was increased*". The results "demonstrate the important effects of the anharmonic terms in the lattice potential energy" (Najmaei et al., 2012)

An "intriguing anomalous behavior" has been observed by Ranjuna and Balakrishnan, 2021, "in the temperature-dependent Raman spectra of mono-, bi-, and trilayer molybdenum disulfide samples *with sulfur vacancies*, measured at high temperatures ranging from room temperature to 463 K". "In contrast to existing reports, [Ranjuna and Balakrishnan] observed a decrease in the FWHM of the A_{1g} phonon mode, along with an increase in the relative intensity of the A_{1g} mode to the E^1_{2g} mode, as the temperature increased. … These observations are explained by considering the presence of *sulfur vacancies*" (Ranjuna and Balakrishnan, 2021).

"Monolayer molybdenum disulfide (MoS_2) … is widely used in a broad range of industries due to its extraordinarily different material properties compared to its bulk counterpart. However, such unique behavior may be greatly affected by its capacity of energy dissipation or *heat conduction*, largely attributed to its inherent phonon scattering properties" (Wang et al., 2023). The phonons of molybdenum disulfide (but this is generally true) "may be greatly affected by parameters such as temperature, defect concentration, etc., reflected by the Raman spectra evolution of A_{1g} or E_{2g} peaks" (Wang et al., 2023).

"Atomically thin molybdenum disulfide (MoS_2) offers potential for advanced devices and *an alternative to graphene* due to its unique electronic and optical properties. The temperature-dependent Raman spectra of exfoliated, monolayer MoS_2 in the range of 100-320 K are reported and analyzed. The linear temperature coefficients of the in-plane $E_{2g}{}^1$ and the out-of-plane A_{1g} modes for both suspended and substrate-supported monolayer MoS_2 are measured. These data, … *enable the thermal conductivity to be extracted*. The resulting thermal conductivity $\kappa = (34.5 \pm 4)$ W/mK at room temperature … , this value is significantly lower than that of graphene" (Yan et al., 2014).

Fano-Raman

Lee et al., 2015, studied Fano resonance and photoluminescence enhancement in monolayer MoS_2 "integrated with plasmonic nanoantenna array". The researchers, "by integrating chemically grown monolayers of MoS_2 with a silver-bowtie nanoantenna array" obtained "a unique two-dimensional optical system". The physical device contains "MoS_2 excitons interacting with the plasmonic resonances of the bowtie array", so that, at low temperatures, the exciton–plasmon coupling results "in a Fano line shape in the reflection spectrum". The Fano line shape "can be tuned by altering the coupling strengths" (Lee et al., 2015). About Raman spectra, see please the Figure 1 in the mentioned reference. There, we can find a SEM image giving the "silver bowtie array directly patterned on well-defined, stacked triangular flakes of mono- and bilayer MoS_2". In Fig.1(c) the Raman spectra of MoS_2, bowtie array, and the bowtie-MoS_2 system are given. The peaks seem being asymmetric.

However, it is in Tanwar et al., 2022, that we can find the "Fano-type wavelength-dependent asymmetric Raman line shapes from MoS_2 nanoflakes". This publication is licensed under CC-BY-NC-ND 4.0. "Excitation wavelength-dependent Raman spectroscopy has been carried out to study electron–phonon interaction (Fano resonance) in multi-layered bulk 2H–MoS_2 nano-flakes. The electron–phonon coupling is proposed to be caused due to interaction between energy of an excitonic quasi-electronic continuum and the discrete one phonon, first-order Raman modes of MoS_2. … Typical wavelength-dependent Raman line shape has been observed, which validates and quantifies the *Fano interaction* present in the samples" (Tanwar et al., 2022). And also: "The experimentally obtained Raman scattering data show very good agreement with the *theoretical Fano–Raman line-shape functions* and help in estimating the coupling strength". The researchers tell that "In *bulk* materials, Fano resonance takes place due to matching of energy of the electronic continuum provided by free carriers via either heavy doping or photoexcited carriers, with the discrete one-phonon energy, causing a constructive and destructive interference" (Tanwar et al., and references therein). The result of the Fano resonance is an asymmetry of the Raman line shape and a shift of the peak. "Another prominent feature of these Raman profiles depicting Fano resonance *is the presence of antiresonance (dip) on either the pre-maximum or post-maximum side* (30) depending on the type of carrier (electron or hole) involved in generating the electronic continuum" (Tanwar et al., 2022, referring to (30) which is Tanwar, et al., 2021).

In the Figure 2 by Tanwar et al., 2022, we can find the Raman spectra of MoS_2 flakes obtained with 633 and 532 nm laser excitations. The quantum confinement is not considered, and the observed asymmetry is ascribed to the Fano interaction. The theoretical fitting is proposed by Tanwar and coworkers in their Figure 3. The line-shape is given in their Eq.3, which is told defining the "Fano–Raman line-shape function". The mentioned reference is Hasdeo et al., 2014. Note please that Tanwar and coworkers are giving the Fano parameter as "q". Here, we use "q" for the Tsallis q-parameter.

In Susmitha et al., 2023, Raman spectroscopy is used to study "phonon softening, surface temperature, Fano resonance, and phase change in MoS_2 nanoflakes". "The phonon softening and asymmetry in the vibrational modes are attributed to the laser-induced heating and Fano resonance, respectively. Fano resonance happens due to electron–phonon coupling and appears as an asymmetry in the Raman line shape." (Susmitha et al., 2023). The Fano line shape is used for fitting.

Appendix – q-Gaussian, split-q-Gaussian and q-BWF functions

The q-Gaussian functions are probability distributions proper of the Tsallis statistics (Tsallis, 1988, Hanel et al., 2009). These functions are based on a generalized form of the exponential function, characterized by a continuous real parameter q. When q is going to 1, the q-exponential becomes the usual exponential function. The value q=2, (Naudts, 2009), corresponds to the Cauchy distribution, also known as the Lorentzian distribution; the q-Gaussian function is therefore a generalization of the Lorentzian distribution too. The change of q-parameter is allowing the q-Gaussian function to pass from the Gaussian to the Lorentzian distribution.

As given by Umarov et al., 2008, the q-Gaussian function is: $f(x) = Ce_q(-\beta x^2)$, where $e_q(.)$ is the q-exponential function and C a scale constant (in the exponent, $\beta = 1/(2\sigma^2)$). The q-exponential has expression: $e_q(u) = [1 + (1-q)u]^{1/(1-q)}$.

To have an asymmetric form of the q-Gaussian function, let us write it in the following manner (the center of the band is at x_o):

$$\text{q-Gaussian} = Cexp_q(-\beta(x-x_o)^2) = C[1-(1-q)\beta(x-x_o)^2]^{1/(1-q)}$$

In ChemRxiv we considered the asymmetric q-Gaussians, as given by Devi (2021):

$$\text{q-Gaussian}_{\text{LEFT}} = Cexp_{q_L}(-\beta_L(x-x_o)^2) = C[1-(1-q_L)\beta_L(x-x_o)^2]^{1/(1-q_L)}, \text{ when } x-x_o < 0$$

$$\text{q-Gaussian}_{\text{RIGHT}} = Cexp_{q_R}(-\beta_R(x-x_o)^2) = C[1-(1-q_R)\beta_R(x-x_o)^2]^{1/(1-q_R)}, \text{ when } x-x_o > 0$$

Parameters q and β of the Left and the Right parts are different. The most proper name for this asymmetric function is split-q-Gaussian. We have also generalized the Breit-Wigner-Fano into a q-Breit-Wigner-Fano.

In Fityk, a q-Gaussian function can be defined in the following manner:

define Qgau(height, center, hwhm, q=1.5) = height*(1+(q-1)*((x-center)/hwhm)^2)^(1/(1-q))

q=1.5 the initial guessed value of the q-parameter. Parameter hwhm is the half width at half maximum of the component. When q=2, the q-Gaussian is a Lorentzian function, that we can find defined in Fityk as:

Lorentzian(height, center, hwhm) = height/(1+((x-center)/hwhm)^2)

When q is close to 1, the q-Gaussian becomes a Gaussian function. The split q-Gaussian is defined as:

Splitqgau(height, center, hwhm1=hwhm, hwhm2=hwhm, q1=1.5, q2=1.5) = x < center ? Qgau(height, center, hwhm1, q1) : Qgau(height, center, hwhm2, q2)

The split Lorentzian is: SplitLorentzian(height, center, hwhm1=hwhm, hwhm2=hwhm) = x < center ? Lorentzian(height, center, hwhm1) : Lorentzian(height, center, hwhm2)

And the q-BWF can be defined as:

Qbreit(height, center, hwhm, q=1.5, xi=0.1) = (1-xi*(q-1)*(x-center)/hwhm)^2 * height*(1+(q-1)^0.5 *((x-center)/hwhm)^2)^(1/(1-q))

And the BWF can be defined as:

Breit(height, center, hwhm, xi=0.1) = (1-xi*(x-center)/hwhm)^2 * height/(1+((x-center)/hwhm)^2)

Using +xi instead of -xi does not change the fitting results in Fityk.

References

1. Bianconi, A. (2003). Ugo Fano and shape resonances. In AIP Conference Proceedings (Vol. 652, No. 1, pp. 13-18). American Institute of Physics.
2. Cao, Z. Y., Hu, J. W., Goncharov, A. F., & Chen, X. J. (2018). Nontrivial metallic state of MoS 2. Physical Review B, 97(21), 214519.
3. Cao, Z. Y., & Chen, X. J. (2019). Phonon scattering processes in molybdenum disulfide. Applied Physics Letters, 114(5).
4. Devi, S. (2021). Asymmetric Tsallis distributions for modeling financial market dynamics. Physica A: Statistical Mechanics and Its Applications, 578, 126109
5. Fabbri, F., Negri, M., Francaviglia, L., Kaplan, D., Swaminathan, V., Salviati, G., & Fontcuberta i Morral., A. (2022). Raman and photoluminescence of MoS2 flakes and pyramids [Data set]. Zenodo. https://doi.org/10.5281/zenodo.5866629
6. Ferrari, A. C., & Robertson, J. (2000). Interpretation of Raman spectra of disordered and amorphous carbon. Physical Review B 61: 14095–14107.
7. Flack, A. (2022). High-Resolution Raman & PL Imaging of MoS2, Application Note. Edinburgh Instruments Ltd.
8. Frisenda, R., Niu, Y., Gant, P., Muñoz, M., & Castellanos-Gomez, A. (2020). Naturally occurring van der Waals materials. npj 2D Materials and Applications, 4(1), 38.

9. Hanel, R., Thurner, S., & Tsallis, C. (2009). Limit distributions of scale-invariant probabilistic models of correlated random variables with the q-Gaussian as an explicit example. The European Physical Journal B, 72(2), 263.

10. Hasdeo, E. H., Nugraha, A. R., Dresselhaus, M. S., & Saito, R. (2014). Breit-Wigner-Fano line shapes in Raman spectra of graphene. Physical Review B, 90(24), 245140.

11. Lee, C., Yan, H., Brus, L. E., Heinz, T. F., Hone, J., & Ryu, S. (2010). Anomalous lattice vibrations of single-and few-layer MoS2. ACS nano, 4(5), 2695-2700.

12. Lee, B., Park, J., Han, G.H., Ee, H.S., Naylor, C.H., Liu, W., Johnson, A.C. and Agarwal, R., 2015. Fano resonance and spectrally modified photoluminescence enhancement in monolayer MoS2 integrated with plasmonic nanoantenna array. Nano letters, 15(5), pp.3646-3653.

13. Lee, J. U., Kim, K., Han, S., Ryu, G. H., Lee, Z., & Cheong, H. (2016). Raman signatures of polytypism in molybdenum disulfide. ACS nano, 10(2), 1948-1953.

14. Lafuente, B., Downs, R. T., Yang, H., & Stone, N. (2015). 1. The power of databases: The RRUFF project. In Highlights in mineralogical crystallography (pp. 1-30). De Gruyter (O).

15. Miroshnichenko, A. E., Flach, S., & Kivshar, Y. S. (2010). Fano resonances in nanoscale structures. Reviews of Modern Physics, 82(3), 2257.

16. Molina-Sánchez, A., & Wirtz, L. (2011). Phonons in single-layer and few-layer MoS 2 and WS 2. Physical Review B, 84(15), 155413.

17. Najmaei, S., Liu, Z., Ajayan, P. M., & Lou, J. (2012). Thermal effects on the characteristic Raman spectrum of molybdenum disulfide (MoS2) of varying thicknesses. Applied Physics Letters, 100(1).

18. Naudts, J. (2009). The q-exponential family in statistical physics. Central European Journal of Physics, 7, 405-413.

19. Negri, M., Francaviglia, L., Kaplan, D., Swaminathan, V., Salviati, G., i Morral, A. F., & Fabbri, F. (2022). Excitonic absorption and defect-related emission in three-dimensional MoS 2 pyramids. Nanoscale, 14(4), 1179-1186.

20. Novoselov, K.S., Geim, A.K., Morozov, S.V., Jiang, D.E., Zhang, Y., Dubonos, S.V., Grigorieva, I.V., & Firsov, A.A. (2004). Electric field effect in atomically thin carbon films. science, 306(5696), pp.666-669.

21. Pawbake, A. S., Pawar, M. S., Jadkar, S. R., & Late, D. J. (2016). Large area chemical vapor deposition of monolayer transition metal dichalcogenides and their temperature dependent Raman spectroscopy studies. Nanoscale, 8(5), 3008-3018.

22. Ranjuna, M. K., & Balakrishnan, J. (2023). High temperature anomalous Raman and photoluminescence response of molybdenum disulfide with sulfur vacancies. Scientific Reports, 13(1), 16418.

23. Sparavigna, A. C. (2023). q-Gaussian Tsallis Line Shapes and Raman Spectral Bands. Int. J. Sciences, 12(3), 27-40, 2023, http://dx.doi.org/10.18483/ijSci.2671 Available at SSRN: https://ssrn.com/abstract=4398623

24. Sparavigna, A. C. (2023). Asymmetric q-Gaussian functions generalizing the Breit-Wigner-Fano functions. Zenodo. https://doi.org/10.5281/zenodo.8356165

25. Sparavigna, A. C. (2024). Graphene and Graphene Oxide (Raman Spectroscopy). ChemRxiv. doi:10.26434/chemrxiv-2024-86stv-v2

26. Susmitha, B., Arjun, K., & Karthikeyan, B. (2023). Raman spectral studies on phonon softening, surface temperature, fano resonance, and phase change in MoS2 nanoflakes. Applied Physics A, 129(4), 309.

27. Suzuki, R., Sakano, M., Zhang, Y.J., Akashi, R., Morikawa, D., Harasawa, A., Yaji, K., Kuroda, K., Miyamoto, K., Okuda, T. and Ishizaka, K., 2014. Valley-dependent spin polarization in bulk MoS2 with broken inversion symmetry. Nature nanotechnology, 9(8), pp.611-617.

28. Tang, C., Liang, L., Zhu, X., Liu, W., Yang, Q., Zhou, X., Yan, L., Tan, W., Lu, M. and Lu, M., 2021. Theoretical

and experimental Raman study of molybdenum disulfide. Journal of Physics and Chemistry of Solids, 156, p.110154.

29. Tanwar, M., Pathak, D.K., Chaudhary, A., Krylov, A.S., Pfnür, H., Sharma, A., Ahn, B., Lee, S. and Kumar, R., 2021. Pseudo-anomalous size-dependent electron–phonon interaction in graded energy band: solving the Fano paradox. The Journal of Physical Chemistry Letters, 12(8), pp.2044-2051.
30. Tanwar, M., Bansal, L., Rani, C., Rani, S., Kandpal, S., Ghosh, T., Pathak, D.K., Sameera, I., Bhatia, R. and Kumar, R., 2022. Fano-type wavelength-dependent asymmetric Raman line shapes from MoS2 nanoflakes. ACS Physical Chemistry Au, 2(5), pp.417-422.
31. Thripuranthaka, M., Kashid, R. V., Sekhar Rout, C., & Late, D. J. (2014). Temperature dependent Raman spectroscopy of chemically derived few layer MoS2 and WS2 nanosheets. Applied Physics Letters, 104(8).
32. Tsallis, C. (1988). Possible generalization of Boltzmann-Gibbs statistics. Journal of statistical physics, 52, 479-487.
33. Umarov, S., Tsallis, C., Steinberg, S. (2008). On a q-Central Limit Theorem Consistent with Nonextensive Statistical Mechanics. Milan J. Math. Birkhauser Verlag. 76: 307–328. doi:10.1007/s00032-008-0087-y. S2CID 55967725.
34. Wang, Q. H., Kalantar-Zadeh, K., Kis, A., Coleman, J. N., & Strano, M. S. (2012). Electronics and optoelectronics of two-dimensional transition metal dichalcogenides. Nature nanotechnology, 7(11), 699-712.
35. Wang, Y., Dai, H., Liu, Z., & Liu, D. (2023). Phonon scattering in monolayer molybdenum disulfide under different defect concentrations based on temperature-dependent Raman spectra. The Journal of Physical Chemistry C, 127(2), 1109-1116.
36. Wieting, T. J., & Verble, J. L. (1971). Infrared and Raman studies of long-wavelength optical phonons in hexagonal Mo S 2. Physical Review B, 3(12), 4286.
37. Wojdyr, M. (2010). Fityk: a general-purpose peak fitting program. Journal of Applied Crystallography, 43(5-1), 1126-1128.
38. Yan, R., Simpson, J.R., Bertolazzi, S., Brivio, J., Watson, M., Wu, X., Kis, A., Luo, T., Hight Walker, A.R. and Xing, H.G., 2014. Thermal conductivity of monolayer molybdenum disulfide obtained from temperature-dependent Raman spectroscopy. ACS nano, 8(1), pp.986-993.
39. Zhao, M., Ye, Z., Suzuki, R., Ye, Y., Zhu, H., Xiao, J., Wang, Y., Iwasa, Y. and Zhang, X., 2016. Atomically phase-matched second-harmonic generation in a 2D crystal. Light: Science & Applications, 5(8), pp.e16131-e16131.